Experimental and numerical investigation of a micro-structured bubble column with chemisorption

Document license:
TAVERNE

DOI:
[10.1016/j.ces.2016.12.035](10.1016/j.ces.2016.12.035)

Document status and date:
Published: 01/09/2017

Document Version:
Publisher's PDF, also known as Version of Record (includes final page, issue and volume numbers)

Please check the document version of this publication:

• A submitted manuscript is the version of the article upon submission and before peer-review. There can be important differences between the submitted version and the official published version of record. People interested in the research are advised to contact the author for the final version of the publication, or visit the DOI to the publisher's website.
• The final author version and the galley proof are versions of the publication after peer review.
• The final published version features the final layout of the paper including the volume, issue and page numbers.

Link to publication

Experimental and numerical investigation of a micro-structured bubble column with chemisorption

Krushnathej Thiruvalluvan Sujatha [a], D. Jain [a], S. Kamath [a], J.A.M. Kuipers [a], Niels G. Deen [b],*
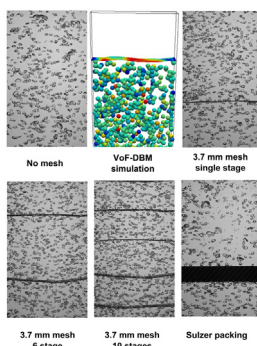
[a] Multiphase Reactors Group, Department of Chemical Engineering and Chemistry, Eindhoven University of Technology, P.O. Box 513, 5600MB Eindhoven, The Netherlands
[b] Multiphase and Reactive Flows Group, Department of Mechanical Engineering, Eindhoven University of Technology, P.O. Box 513, 5600MB Eindhoven, The Netherlands

HIGHLIGHTS

- Wire meshes with 3.7 mm mesh opening has a cutting behavior comparable to Sulzer static mixer (SMV).
- Six mesh stages has a better performance than a single mesh, due to increase in gas holdup and bubble cutting.
- VoF-DBM simulations are validated for superficial gas velocities up to 25 mm/s.

GRAPHICAL ABSTRACT

ABSTRACT

A novel micro-structured bubble column reactor (MSBC) is studied by a combined experimental and simulation approach, for the chemisorption of CO_2 into NaOH. To understand the reactor behavior different reactor configurations are tested for chemisorption by varying the internals (single wire mesh, staged wire meshes, Sulzer packing). Bubble size distribution, pH and holdup data are obtained from chemisorption experiments using an advanced digital image analysis technique. The effect of superficial gas velocities ranging from 5 to 25 mm/s and varying number of wire mesh stages (1, 6 and 10) is deduced from the experiments. The experimental results are used for the validation of the detailed VoF-DBM simulations.

© 2017 Elsevier Ltd. All rights reserved.

1. Introduction

Bubble columns are often used in the chemical industry for gas-liquid contacting processes. For instance, in gas-treating processes to remove H_2S and/or CO_2. The limiting step in the chemisorption process is usually the mass transfer from the gas phase to the liquid phase. The mass transfer rate is a function of the interfacial area, the intrinsic mass transfer coefficient and the driving force. The mass transfer rate can be increased by increasing the interfacial area and/or the interfacial mass transfer coefficient. This can achieved by means of adding internals such as sieve plates, porous plates, and static mixers (SMV) (Baird, 1992; Deen et al., 2000). The addition of internals is known to reduce the back-mixing in the bubble column reactor, which can be advantageous in some

* Corresponding author.
  E-mail address: N.G.Deen@tue.nl (N.G. Deen).

Nomenclature

Dimensionless numbers
Re	Reynolds number
Sc	Schmidt number
Sh	Sherwood number

Greek symbols
μ	dynamic viscosity, [kg·m^{-1}·s^{-1}]
ρ	density, [kg·m^{-3}]
ε	holdup, [–]

Variables
A	area, [m^2]
D	depth, [m]
d	diameter, [m]
d_{32}	Sauter mean diameter, [m]
E	enhancement factor, [–]
F	color function
H	height, [m]
h	height of gas-liquid dispersion, [m]
k_l	mass transfer coefficient, [m·s^{-1}]
N_S	number of species
V	volume, [m^3]
v	velocity, [m·s^{-1}]
W	width, [m]

Y_j	mass fraction of species j
PDF	probability density function, [1/mm]

Sub/superscripts
0	initial
b	bubble
eq	equivalent
f	final
g	gas
H	height expansion
k	index
l	liquid
w	solid wire-mesh
j	species index

Abbreviations
CO_2	carbon-dioxide
NaOH	sodium hydroxide
DBM	discrete bubble model
DIA	digital image analysis
MSBC	micro-structured bubble column
SMV	Sulzer static mixer
VoF	volume of fluid

situations. In our previous work, we have proposed a novel micro-structured bubble column (MSBC) reactor with wire-meshes as internals (Sujatha et al., 2015; Jain et al., 2013; Jain et al., 2014). Jain et al. (2013, 2014) have developed a combined VoF-DBM model to simulate and study the effect of wire mesh in the MSBC reactor. Sujatha et al. (2015) have done experiments in laboratory scale MSBC reactor to study the effect of wire mesh configuration and superficial gas velocity. Three hydrodynamic regimes were identified for bubbly flow in a MSBC with wire mesh in an air-water system for superficial gas velocities in the range of 5–50 mm/s.

The scope of the current paper is to extend the work for the chemisorption of CO_2 into a NaOH solution, by a combined experimental and simulation approach. Bubble size distribution, pH and holdup data are obtained from chemisorption experiments. These data are compared with simulation results obtained from a detailed VoF-DBM model developed by Jain et al. (2014). The effect of the mesh configuration is investigated by varying the mesh opening and the distance between mesh stages for superficial gas velocities ranging from 5 to 25 mm/s.

This paper is organized as follows. The description of the experimental setup and methods used for obtaining the results (i.e. digital image analysis technique and VoF-DBM method) are discussed elaborately. The results and discussion section consists of visual analysis, experimental results and comparison of experiments with simulation.

Table 1
Overview of different wire meshes used for experiments.

Mesh #	Wire diameter (mm)	Mesh opening (mm)	Open area (%)
4	0.80	5.6	76
6	0.55	3.7	76
6	0.90	3.3	62
8	0.50	2.7	71
10	0.31	2.2	75
12	0.31	1.8	73
18	0.22	1.2	71

2. Material and methods

A flat pseudo-2D bubble column reactor of dimensions (width W = 200 mm, depth D = 30 mm, height H = 1300 mm) is chosen for experiments. The reactor walls are constructed of transparent glass to enable visual observation by the eye or using a camera. The gas is fed into the column via a group of fifteen gas needles centrally arranged in the distributor plate. The needles have a length (L) = 50 mm, inner diameter (I.D.) = 1 mm and outer diameter (O.D.) = 1.5875 mm. The needles extend 10 mm above the bottom plate and are spaced with a center-to-center distance of 9 mm. An array of five needles is classified as a group, and each group of needles is connected to a mass flow controller. Subsequently, three mass flow controllers are used to control the gas flow rates in the column. Micro-structuring in the reactor is realized by means of thin wires of various dimensions arranged in a mesh structure or by using a Sulzer packing (SMV). The wire mesh or Sulzer packing can be mounted onto the column by using a modular insert, designed for this purpose. The modular insert design allows full flexibility to attach one or more wire meshes at different locations of the insert. The dimensions of the column including the insert are as follows: width = 140 mm, depth = 30 mm, height = 1300 mm. The location of the wire mesh was fixed for the experiments at a distance of 260 mm from the bottom distributor plate and the Sulzer packing is fixed at 240–260 mm. An overview of the several mesh configurations can be seen in Table 1.

The experimental procedure followed for the CO_2−NaOH system is as follows. The column is filled with a well stirred solution of sodium hydroxide prepared with pH 12.5. Inert gas nitrogen is used to aerate the column before the starting time of the experiment at desired gas flow rate. The camera is focused to a particular section of the column to capture sharp images. The pH meter is immersed in the NaOH solution, at the top of the column to measure and record local pH for the duration of reaction. The flow is switched to CO_2 and the timer is started. Initial liquid height is noted down at time t = 0 and the high-speed recording of images is started. As the reaction proceeds the change in height of
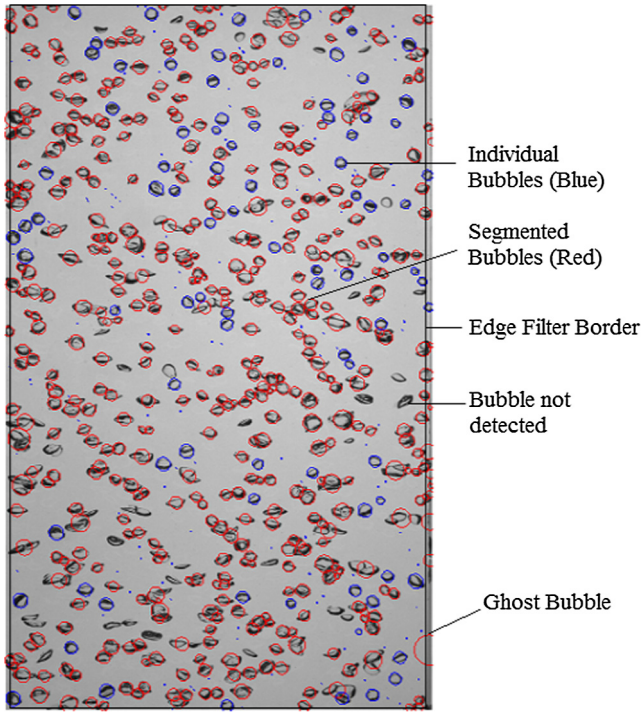
Fig. 1. Image after detection. Individual bubbles are indicated by blue circles and segmented bubbles are indicated by red Carbon conversioncircles.

gas-liquid dispersion is noted down. Once there is no relevant change in pH with time the CO_2 flow is switched back to nitrogen flow. The change in the gas holdup is observed via the change in height of the gas-liquid dispersion with time.

2.1. Digital image analysis

The DIA technique (Lau et al., 2013a; Lau et al., 2013b) was developed to determine the mean diameter d_{eq}, bubble size distributions and gas holdup in pseudo-2D bubble column reactor. Sujatha et al. (2015) improved the DIA technique to detect very small bubbles. The image analysis algorithm has four main operations: (a) Image filtering (b) separation of bubbles into solitary and overlapping bubbles (c) segmentation of overlapping bubbles using watershedding technique (d) combination of solitary and overlapping bubble images. Image filtering involves operations to obtain a desired image involving removal of the inhomogeneous illumination using an Otsu filter (Otsu, 1975). The Otsu filter determines the threshold for separating the bubbles from the background, by thresholding individual blocks of an image. The edges of the bubbles are detected by a Canny edge detection algorithm. The bubbles are separated into solitary bubbles and overlapping bubbles using roundness as a separation criteria. The images with solitary bubbles are segmented by marking the bubbles, whereas the overlapping bubbles are segmented using the watershed algorithm proposed by Meyer (1994). An example image after bubble detection is shown in Fig. 1. In DIA technique, errors can occur due to different sources such as: imaging error, filtering errors, separation errors, segmentation error and computational error. The measurement accuracy of DIA is estimated by using artificial images as elaborately discussed in the work of Lau (Lau et al., 2013a; Lau et al., 2013b). For objects between 10–30 pixels, the maximum and minimum errors are estimated to be +2% and −6% respectively. For objects greater than 30 pixels, the error is estimated to be between +0.5% and −1.0%.

A CMOS camera with resolution of 2016 *pixel* × 2016 *pixel* is used to capture the images of two-phase bubbly flow by using back-lighting to obtain maximum contrast between the bubbles and the background. The MSBC is divided into three different sections for the purpose of imaging and 4000 images are made at 50 Hz for each section. Images from each section have a size of 210 mm × 140 mm and a small overlap of 40 mm. The resolution of the image is 0.11 mm/pixel.

The Sauter mean diameter of an image is calculated from the equivalent diameter using the following equation:

$$d_{32} = \frac{\sum_{k=0}^{n} d_{eq,k}^3}{\sum_{k=0}^{n} d_{eq,k}^2} \tag{1}$$

The probability density function (PDF) for a particular bubble diameter class is the ratio of number of bubbles in a particular diameter class (Δd_{eq}) to the sum of number of bubbles in all size classes. Therefore, the PDF of a particular size class (Δd_{eq}) is calculated from the number of bubbles and average bubble diameter as follows:

$$PDF_{\Delta d_{eq}} = \frac{N_{\Delta d_{eq}}}{\left(\sum_{\Delta d_{eq,min}}^{\Delta d_{eq,max}} N_{\Delta d_{eq,k}}\right) \Delta d_{eq}} \tag{2}$$

The gas holdup is determined for the air-water system by liquid expansion measurements. It is calculated by the following formula:

$$\varepsilon_{(g,H)} = \frac{h_f - h_0}{h_f} \tag{3}$$

where h_f is the height of the gas-liquid dispersion and h_0 is the initial height of the liquid.

3. Volume of fluid - discrete bubble model

A Volume of Fluid (VoF) - Discrete Bubble Model (DBM) is used to model the hydrodynamics of the system. This model is an Euler-Lagrangian model. The bubbles are tracked and the liquid phase is treated as a continuum. A force balance is solved for every bubble using Newton's second law of motion. For an incompressible bubble the equations are given by:

$$\rho_b \frac{d(V_b)}{dt} = (\dot{m}_{l \to b} - \dot{m}_{b \to l}) \tag{4}$$

$$\rho_b V_b \frac{d(\mathbf{v})}{dt} = \Sigma \mathbf{F} - \left(\rho_b \frac{d(V_b)}{dt}\right)\mathbf{v} \tag{5}$$

$$\Sigma \mathbf{F} = \mathbf{F_G} + \mathbf{F_p} + \mathbf{F_D} + \mathbf{F_L} + \mathbf{F_{VM}} + \mathbf{F_W} \tag{6}$$

The forces considered on the bubble are due to gravity ($\mathbf{F_G}$), local pressure gradients ($\mathbf{F_p}$), liquid drag ($\mathbf{F_D}$), lift forces($\mathbf{F_L}$), virtual mass forces($\mathbf{F_{VM}}$) and wall forces ($\mathbf{F_W}$). Closures for these forces are given in the work of Jain et al. (2013).

3.1. Fluid phase hydrodynamics

The whole system is divided into four phases, each with its own volume fraction (ε): (a) liquid (ε_l), (b) bubble (ε_b), (c) gas (ε_g, continuous layer above the liquid height), and (d) wire-mesh (ε_w solid). where the sum of all volume fractions equals unity:

$$\varepsilon_l + \varepsilon_g + \varepsilon_b + \varepsilon_w = 1 \tag{7}$$

The liquid phase hydrodynamics is described by the volume averaged Navier-Stokes equations, which consists of continuity and momentum equations:

$$\frac{\partial(\rho_f \varepsilon_f)}{\partial t} + \nabla \cdot (\varepsilon_f \rho_f \mathbf{u}) = (\dot{M}_{b \to l} - \dot{M}_{l \to b}) \tag{8}$$
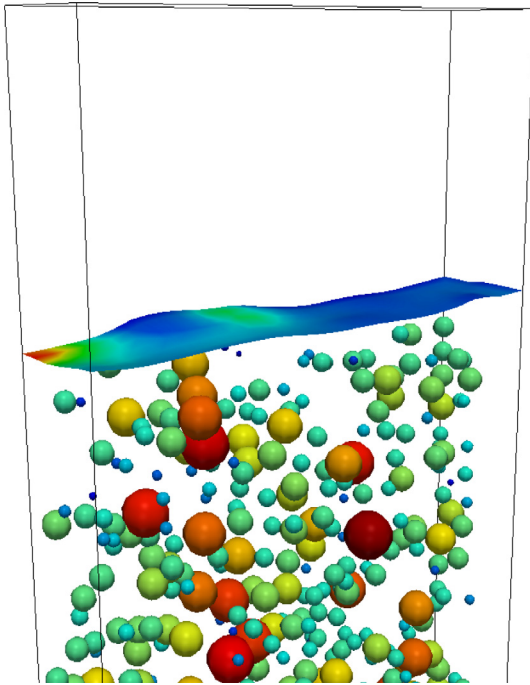
Fig. 2. Example snapshot of VoF-DBM simulation showing bubbles and free surface.

$$\frac{\partial}{\partial t}(\rho_f \varepsilon_f \mathbf{u}) + (\nabla \cdot \varepsilon_f \rho_f \mathbf{u}\mathbf{u}) = -\varepsilon_f \nabla p + \rho_f \varepsilon_f \mathbf{g} - \mathbf{f}_\sigma - \mathbf{f}_{l\rightarrow b} + \mathbf{f}_{w\rightarrow l}$$
$$+ \left\{ \nabla \cdot \varepsilon_f \mu_{eff} \left[((\nabla \mathbf{u}) + (\nabla \mathbf{u})^T) - \frac{2}{3}\mathbf{I}(\nabla \cdot \mathbf{u}) \right] \right\}$$
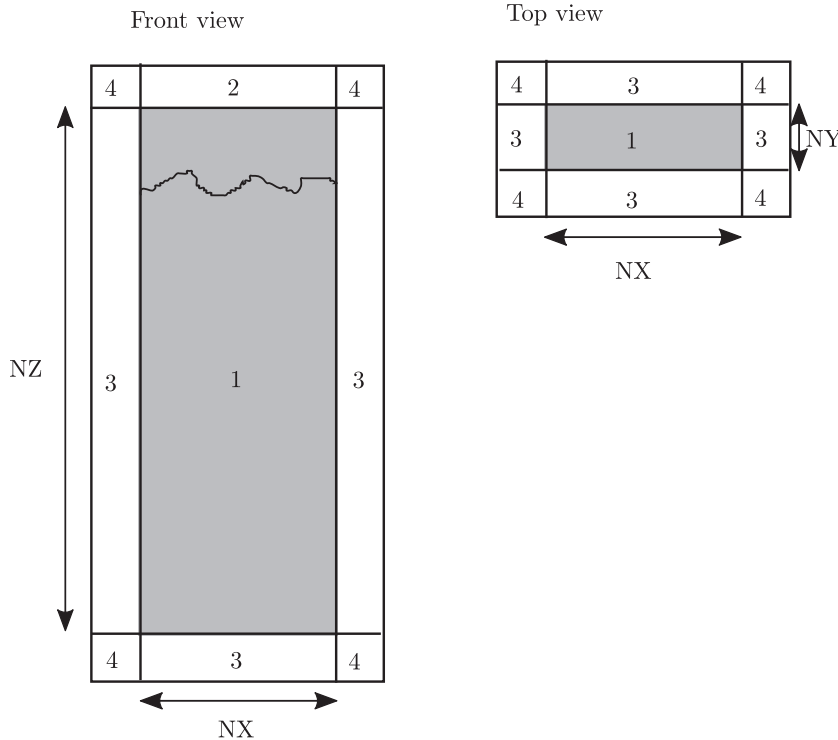
$$(9)$$

where

Table 2
Flag meaning for cell boundary conditions.

Flag	Boundary conditions
1	Interior cell, none specified
2	Prescribed pressure cell, free slip
3	Impermeable wall, no slip, Neumann conditions for species
4	Corner cell, none specified

$$\varepsilon_f = \varepsilon_l + \varepsilon_g \tag{10}$$

$$\mu_{eff} = \mu_{L,l} + \mu_{T,l} \tag{11}$$

$\dot{M}$ represents the rate of mass transfer. $\mathbf{f}_\sigma$ represents the local volumetric surface tension force acting on the free surface at the top of the column and $\mathbf{u}$ represents the average fluid velocity. The interface can be seen in Fig. 2.

A Volume of Fluid (VoF) method is used to simulate the free surface and the gas above the liquid level in the column. van Sint Annaland et al. (2005) have used this method to successfully show the coalescence of two gas bubbles in a fluid. The grid size used here is larger compared to direct numerical simulations but this is acceptable as the surface only has a small curvature. The local average ρ and μ are calculated using a color function F which is governed by:

$$\frac{DF}{Dt} = \frac{\partial F}{\partial t} + (\mathbf{u} \cdot \nabla F) = 0 \tag{12}$$

$$F = \frac{\varepsilon_l}{\varepsilon_l + \varepsilon_g} = \frac{\varepsilon_l}{\varepsilon_f} \tag{13}$$

It can be easily noted that the grid cells lying completely below the free surface have $\varepsilon_g = 0$ and similarly the grid cells lying completely above the free surface have $\varepsilon_l = 0$. The properties like density and viscosity for the other grid cells that cover the free surface are calculated as follows.

Fig. 3. Boundary conditions for the VoF-DBM; Front view at $j = $ NY/2 and top view for cells $k = 2$ to $k = $ NZ-1.

$$\rho_f = F\rho_l + (1 - F)\rho_g \tag{14}$$

$$\frac{\rho_f}{\mu_f} = F\frac{\rho_l}{\mu_l} + (1 - F)\frac{\rho_g}{\mu_g} \tag{15}$$

The boundary conditions are applied using a flag matrix concept. Fig. 3 shows the different values of the flags of the pseudo 2-D column. The cells are assigned different flag values indicating different types of boundary conditions that are listed in Table 2.

The turbulence in the liquid phase due to bubbly flow is taken into account by using a sub-grid scale model proposed by Vreman (2004) for the eddy viscosity.

Bubble coalescence is accounted based on the model proposed by Sommerfeld et al. (2003). The collision time is determined by the relation reported by Allen and Tildesley (1989). Film drainage time for coalescence to occur is calculated based on the model of Prince and Blanch (1990). When the contact time is less than the film drainage time coalescence does not occur and the bubbles simply bounce. Otherwise, they coalesce. A detailed description of the model can be found in Darmana et al. (2005). Bubble breakup occurs if the inertial force exceeds the surface tension forces, the ratio of which can be represented as Weber number. The critical Weber number for breakup to occur is 12 as determined by Jain et al. (2014). Based on this, a binary breakup model is modeled in which the bigger bubble is placed at the position of the parent bubble and the smaller bubble is placed randomly around the centroid of the bigger bubble.

3.2. Wire-mesh and cutting

The wire mesh is present in the middle of the column to cut the bubbles. A simple geometric cutting model proposed by Jain et al. (2013) is incorporated to account for cutting the bubbles when they pass the wire mesh. A stochastic factor called cutting efficiency is introduced into the model to characterize the fraction of bubbles that is actually cut by the wire mesh. A cutting efficiency 0 means there is no cutting and a value of 1 means all bubbles are eligible to get cut. The drag that the wire-mesh exerts on the liquid is taken into account in Eq. (9) (Jain et al., 2013).

3.3. Chemical species equations

The species are accounted by Y_j which is the mass fraction of species j. Species balance for $N_s - 1$ components are solved simultaneously with appropriate boundary conditions, where N_s is number of components present in the system. The fraction of the last component can be derived from the overall mass balance.
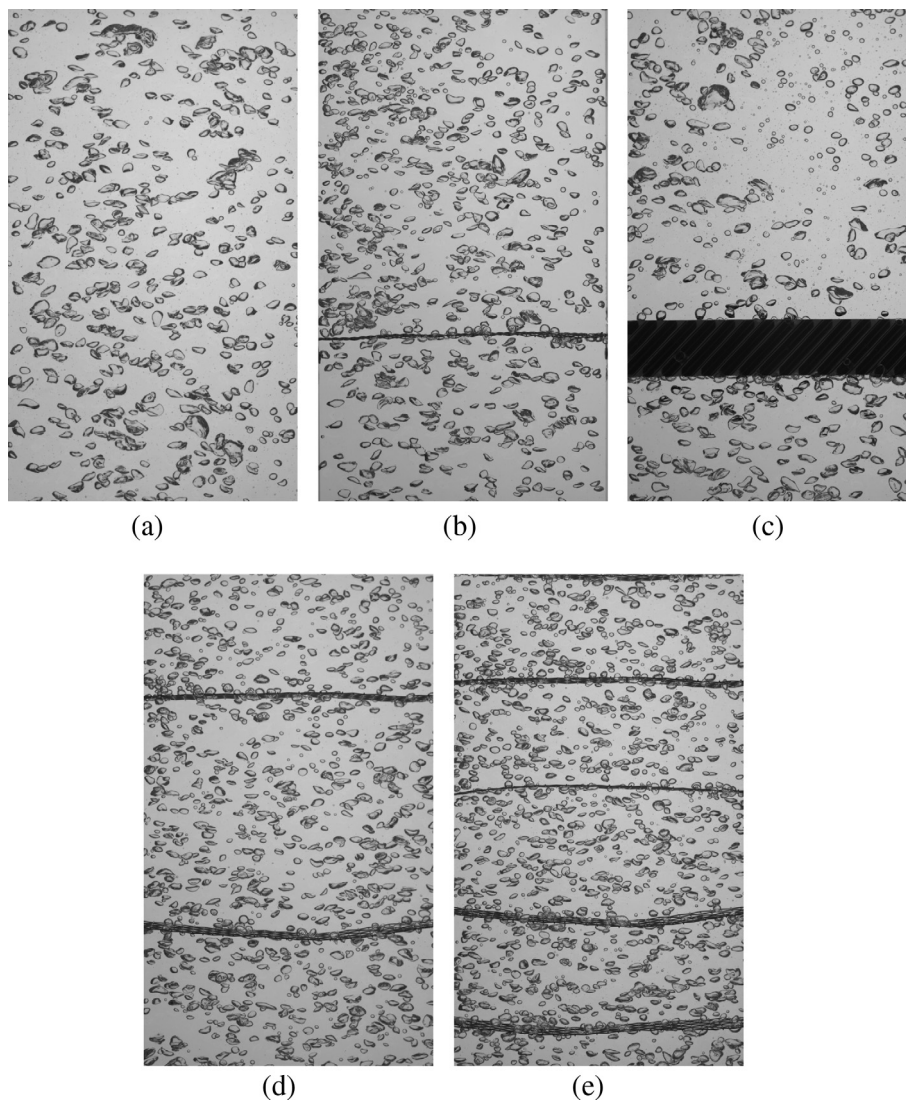

Fig. 4. Images of bubbly flow in the MSBC at a superficial gas velocity of 15 mm/s: (a) no mesh, (b) mesh opening 3.7 mm, (c) Sulzer packing, (d) 6 stage and (e) 10 stages.

$$\frac{\partial}{\partial t}\left(F\varepsilon_f\rho_f Y_j\right) + \nabla\cdot\left(F\varepsilon_f\left(\rho_l\mathbf{u}Y_j - \Gamma_{j,eff}\nabla Y_j\right)\right) = \left(\dot{M}^j_{b\to l} - \dot{M}^j_{l\to b}\right) + F\varepsilon_f S_{Rj} \tag{16}$$

$$\sum_{j=1}^{N_S} Y_j = 1 \tag{17}$$

S_{Rj} is the source term accounting for the production or consumption of species j due to chemical reaction.

The mass transfer is given by:

$$\dot{m}^j_b = Ek^j_l A_b \rho_l (Y^{j*}_l - Y^j_l) \tag{18}$$

where the mass transfer coefficient k_l is calculated through a Sherwood correlation. Several mass transfer correlations are available in literature for bubbly flows. Brauer (1981) gives a correlation for ellipsoidal bubbles accounting for the shape of the bubble due to the deformations caused by liquid flow around bubbles:

$$Sh = 2 + 0.015 \times Re_B^{0.89}Sc^{0.7} \tag{19}$$

The correlation for the enhancement factor (E) provided by Westerterp et al. (1987) is used as proposed by Darmana et al. (2005).

4. Results

4.1. Visual observation

Images are obtained using a high-speed camera operated at 50 Hz, for a velocity of 5–30 mm/s for different wire meshes and the Sulzer packing (SMV). Fig. 4 shows the images of bubbly flow in a MSBC for different configurations, such as no internals, with mesh (single 3.7 mm mesh opening, 3.7 mm mesh in six stages and 3.7 mm mesh in 10 stages) and Sulzer packing. The images are shown for the mid section at a superficial gas velocity of 15 mm/s. In Fig. 4, there are small bubbles present above and below the mesh or Sulzer packing. The presence of small bubbles also increases with increasing superficial gas velocities as a consequence of bubble break-up. In Fig. 4a, for the case without internals the bubbles are homogeneously distributed in the column with some big bubbles. When comparing the different images in Fig. 4, it can be seen qualitatively that the bubble cutting occurs in the presence of internals.
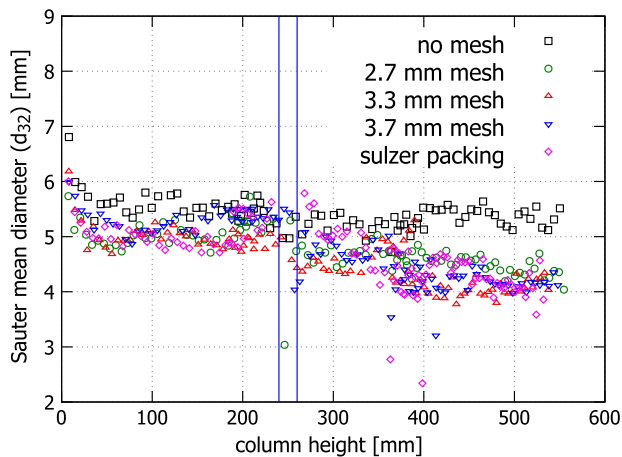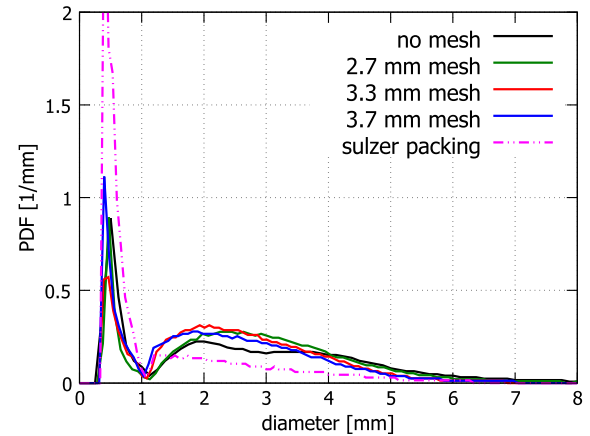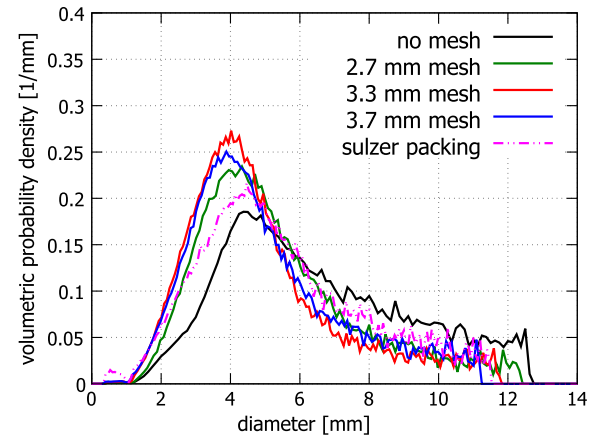

Fig. 5. Sauter mean bubble diameter vs height for varying mesh types at superficial gas velocity 25 mm/s. The positions of the mesh [260 mm] and the packing [240–260 mm] are indicated by the solid lines.

(a)

(b)

Fig. 6. Effect of varying mesh types on bubble size distribution at superficial gas velocity 25 mm/s in the top section [420–600 mm] based on: (a) number density (b) volumetric probability density.
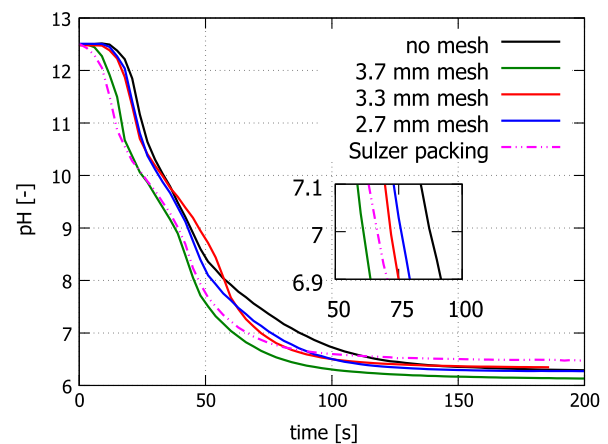

Fig. 7. pH vs time curve for different mesh types at superficial gas velocity 25 mm/s.

4.2. Effect of internals

It is important to note that for Figs. 5 and 6, time-averaging is done for a duration of 4 s (i.e. between 10 and 14 s after the CO_2 flow starts in the column) for all superficial gas velocities and mesh openings. The width of the averaging window is chosen such that the pH and bubble size remains constant. The chemisorption of

CO_2 into NaOH starts immediately when the gas is switched from N_2 to CO_2 and this causes the bubble size to decrease rapidly for 10 s. Hence, the averaging is done from 10 to 14 s, as it is reasonable to assume that the hydrodynamics of the bubbly flow does not change within such a short time span as there is a very small change in pH. This assumption enables comparison of the cutting behavior of different internals at a particular superficial gas velocity.

The effect of mesh configuration is studied for three different wire mesh openings (i.e. for 2.7 mm, 3.3 mm and 3.7 mm) for comparison with the no mesh case and Sulzer packing. The time-averaged Sauter mean diameter and volumetric probability density function are plotted in Figs. 5 and 6 respectively. The Sauter mean diameter is ratio of volume to surface area of the detected bubbles from the three different image sections. It is used to evaluate the mass transfer performance of the wire meshes/packing used in the MSBC.

Fig. 5 shows the time averaged Sauter mean diameter plotted vs height of the MSBC, for different configurations of internals. The meshes/packings perform much better than the no mesh case, as there is approximately 1 mm drop in bubble diameter after the location of mesh/packing (i.e. 260 mm).

The bubble cutting is also evident in Fig. 6, which shows the time-averaged volumetric probability density vs diameter for different column configurations. Sulzer packing performs the best in terms of resizing the bubbles. Amongst the wire meshes the mesh with 3.7 mm opening performs the best.

This can also be observed in the plot of pH vs time for different cases as shown in Fig. 7, as the pH curve for the 3.7 mm mesh opening and Sulzer packing drops fast to reach pH 7 in 70 s. The MSBC with no mesh configuration takes almost 90 s for reaching pH 7 at same velocity. Hence the pH decay curves show that MSBC with internals perform much better than the configuration with no internals for a reaction limited by gas-liquid mass transfer. It should be observed that although Sulzer packing has better cutting than the 3.7 mm mesh it has a similar performance in terms of mass transfer.

4.3. Effect of superficial gas velocity

The effect of superficial gas velocity on the time-averaged bubble size distribution can be seen in Fig. 9. At 5 mm/s, two peaks can be observed. The left peak corresponds to very small bubbles (less than 1 mm in diameter) and the larger peak corresponds to the average bubble size (3 mm diameter). The bimodal nature of distribution is due to the formation of very small bubbles resulting from
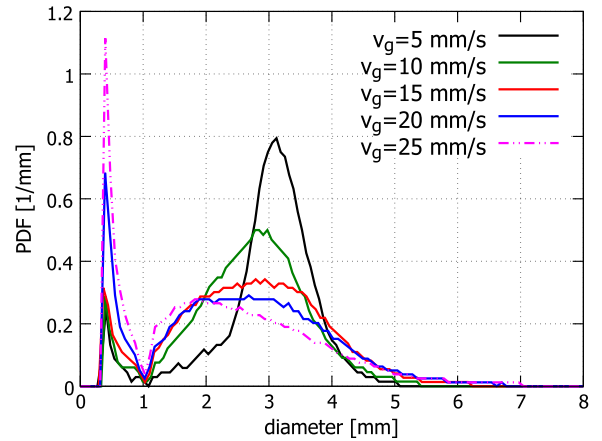

Fig. 9. Bubble size distribution with varying superficial gas velocities [5–25 mm/s] for mesh opening 3.7 mm in the top section [420–600 mm].
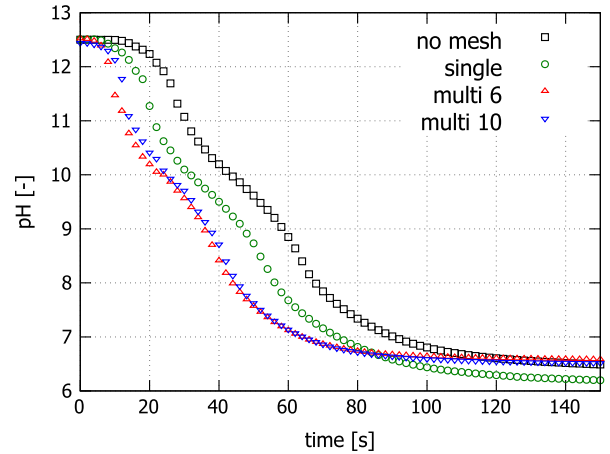

Fig. 10. pH vs time curve at a superficial gas velocity of 20 mm/s with varying mesh stages for a mesh opening of 3.7 mm.
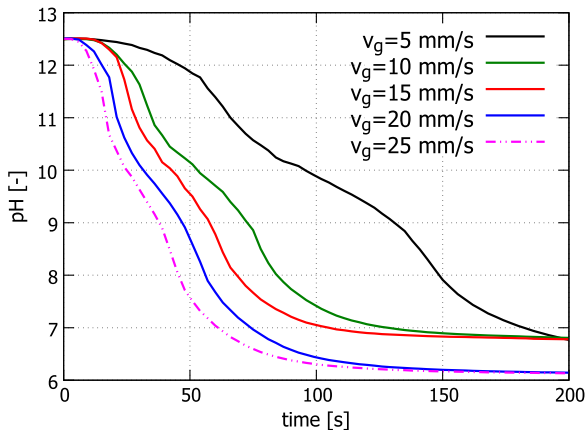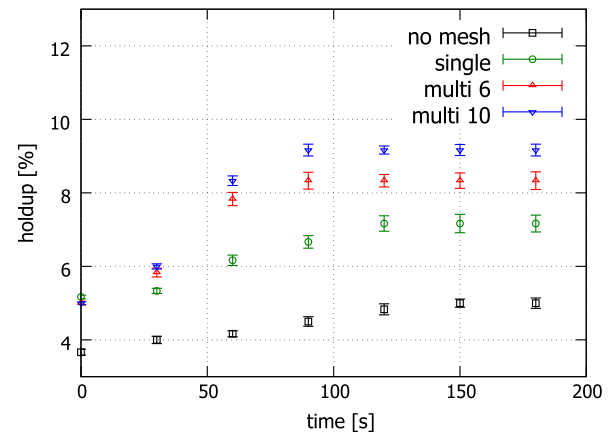

Fig. 11. Gas holdup vs time curve at a superficial gas velocity of 20 mm/s with varying mesh stages for a mesh opening of 3.7 mm.

breakup at the free surface, which are subsequently dragged down into the column by liquid circulation. It can be seen that as the velocity is increased, the distribution becomes flatter due to bubble coalescence and breakup until 15 mm/s. For higher velocities, the distribution of the second peak tends to shift towards smaller bubbles as a result of enhanced bubble cutting and breakup. However,

Fig. 8. pH vs time curve with varying superficial gas velocities [5–25 mm/s] for mesh opening 3.7 mm.

with the presence of internals the bubble cutting has an added impact on the bubble size distribution. The rate of pH decay with increasing superficial gas velocities can be seen in Fig. 8.

4.4. Effect of reactor staging

It is observed that in the single mesh configuration, large bubbles are cut by the mesh but they re-coalesce above the mesh. Stacking multiple meshes enables successive cutting of those large bubbles. Moreover, as the number of meshes increases, the liquid back-mixing reduces significantly. The spacing between successive meshes controls the circulation patterns and the reactor displays more of a plug flow behavior as the mesh spacing is reduced.

Two multiple mesh configurations with six and ten mesh stages are tested by chemisorption experiments for the mesh with mesh openings of 3.7 mm. The reactor with six meshes has a better performance as seen in Fig. 10, from the pH decay curves, as compared with the no mesh and single mesh configurations. Increasing the number of meshes to ten, does not have a significant effect on the pH decay curves, as back-mixing is reduced due to a small spacing between consecutive mesh stages in this configuration.

The trends in the gas holdup profiles are similar, as seen in Fig. 11. In all cases, the gas holdup profiles show an increase over time. The gas holdup for the multiple mesh cases are much higher in comparison with the no mesh and single mesh cases, mainly due to the large amount of bubble cutting occurring in the column. The reduction in bubble size leads to an increased bubble residence time. The bubbles are also decelerated due to the significant hydrodynamic resistance offered by the multiple mesh stages. Henceforth, this leads to a notable increase in the gas holdup in for the multiple-mesh configuration. The high gas holdup explains the poor performance of the ten-mesh configuration, as bubble swarm effects can also lead to a reduction in the mass transfer rates. Therefore the combined effect of back-mixing and swarm effects

counteracts the advantages offered by the reduced bubble sizes in the ten-mesh configuration. This explains the comparable performance of the six-mesh and ten-mesh configuration in terms of pH decay.

4.5. Comparison of experiments with VoF-DBM simulation

4.5.1. Single mesh configuration

Simulations were conducted for five superficial gas velocities (5, 10, 15, 20, 25 mm/s) to compare with experiments carried out with a wire mesh of 3.7 mm opening. The mesh was placed at a height of 260 mm from the bottom. Jain et al. (2015) have determined that the cutting efficiency $\geqslant 0.01$ has no significant effect on the mean bubble diameter and gas holdup. Therefore, a cutting efficiency of 0.1 was used for the simulations. The results of Sauter mean diameter, bubble size distribution, pH and gas holdup will now be discussed for a superficial gas velocity of 15 mm/s.

Fig. 12a shows the comparison of the Sauter mean diameter between experiments and VoF-DBM simulations. The nature of the cutting in the model of Jain et al. (2013) is abrupt and occurs for all cases (initial bubble diameter = 4 mm, 5 mm and 6 mm), whereas in experiments the cutting is gradual. The discrepancy between experiments and simulations is due to under-prediction of breakup rates or over-prediction of the bubble coalescence rates in the simulations. A sensitivity analysis of the coalescence and breakup parameter is beyond the scope of this paper.

A comparison of the bubble size distributions is shown in Fig. 12b. It can be seen that the first peak of the experiments is not well captured in the simulations, as we do not model the violent breakup at the top interface. Experiments cannot detect bubbles below 0.3 mm whereas the simulation can keep track of these very small bubbles, resulting in a smoother initial curve in the simulations. However, the simulation captures the overall trend of the experiments fairly well.
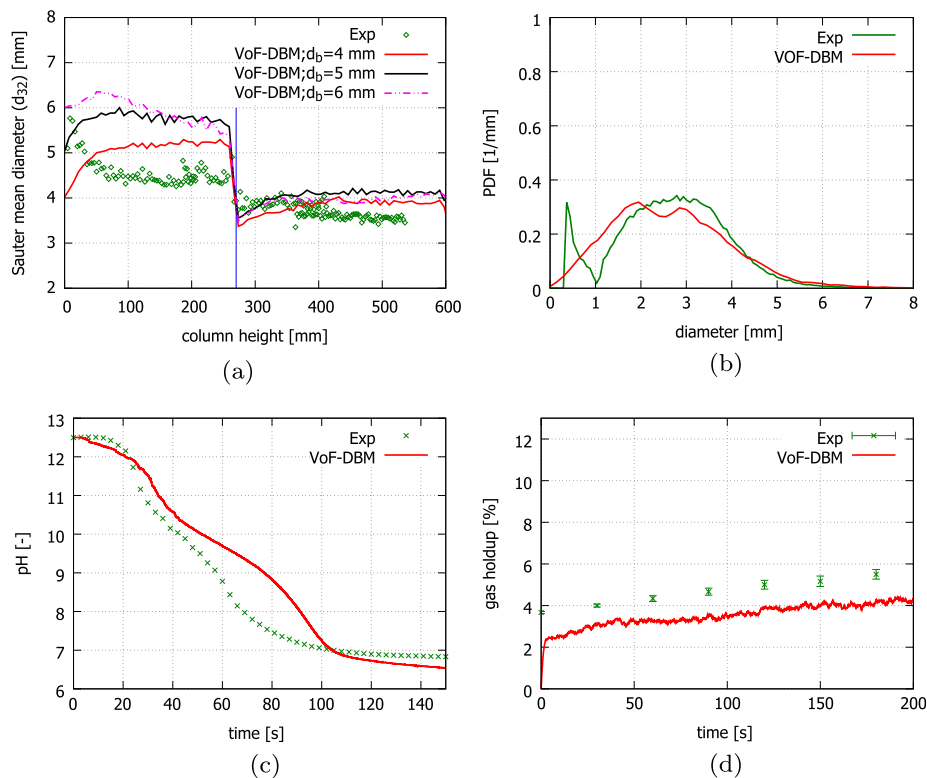

Fig. 12. Behavior of the system with a mesh opening of 3.7 mm and a superficial gas velocity of 15 mm/s: (a) Sauter mean diameter [time averaged]. The location of the mesh at 260 mm is indicated by the solid line (b) bubble size distribution [time averaged] in the top section [420–600 mm] (c) pH vs time (d) gas holdup vs time.
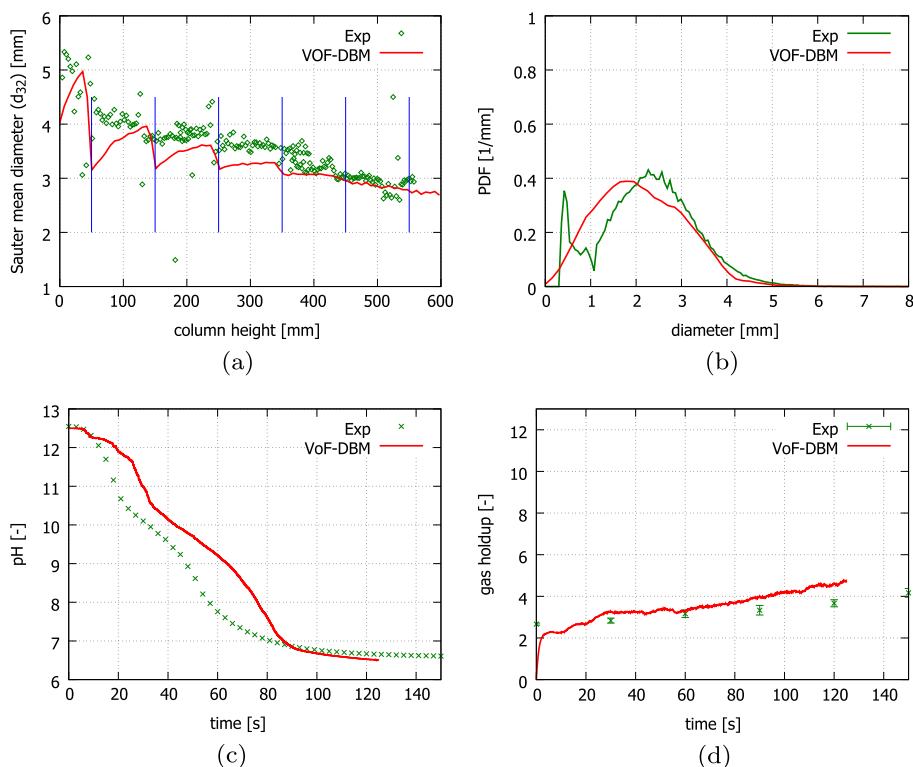
Fig. 13. Behavior of the system with a mesh opening of 3.7 mm, 6 stages and a superficial gas velocity of 15 mm/s: (a) Sauter mean diameter [time averaged]. The location of the meshes are indicated by solid lines at 50, 150, 250, 350, 450, 550 mm respectively. (b) bubble size distribution [time averaged] in the top section [420–600 mm] (c) pH vs time (d) gas holdup vs time.

Fig. 12c shows a comparison of the pH histories obtained experimentally and numerically. It can be seen that the two inflection points are well matched, which indicates that the reaction kinetics are a good description of reality. But the model under-predicts the pH decay rate. This could be due to the presence of large bubbles which in turn lead to lower rate of mass transfer. The time taken for neutralization (pH 7) is well captured by the model as seen in Fig. 12c.

The gas holdup values match well between experiments and simulations as the error stays below 10% for all cases, except at time $t = 0$ (as shown in Fig. 12d). The holdup predicted by simulations is lower than the experimentally determined value at time $t = 0$, as a result of the differences in the startup procedure for chemisorption. In simulations, the hydrodynamics calculations are performed for a N_2–NaOH system until numerical effects disappear and then the system is switched to chemisorption at time $t = 0$. The gas in reactor is completely switched to CO_2 and it reacts with NaOH, leading to disappearance of bubbles throughout the reactor. This causes a decrease in the gas holdup at the onset of chemisorption. However, in the experiments few N_2 bubbles are still present in the bubble column after startup in addition to CO_2 gas. As the N_2 bubbles do not react with NaOH, they have an added contribution to the gas holdup until they leave the column. The deviation in gas holdup predicted by simulations and experiments remains approximately constant (for $t > 0$) as seen in Fig. 12d.

4.5.2. Multiple-mesh configuration: six stages

Simulations were conducted for three superficial gas velocities [15, 20, 25 mm/s] to compare with experiments performed with a six stage multiple-mesh configuration using a mesh opening of 3.7 mm. The first mesh was placed at a distance of 50 mm from the bottom and the spacings between consecutive meshes were

0.10 m. A cutting efficiency of 0.1 was used for the simulations. The results of the Sauter mean diameter, bubble size distribution, pH and gas holdup will now be discussed for a superficial gas velocity of 15 mm/s.

The Sauter mean diameter is well captured by the simulations as seen in Fig. 13a. An initial bubble diameter of 4 mm is used in the simulations, whereas a narrow bubble size distribution is generated during the experiments. This explains the mismatch in the Sauter mean diameter at the bottom of the column. In general, the cutting model predicts the overall trend of the Sauter mean diameter with good accuracy for the multiple-mesh configuration.

Fig. 13b compares the measured and simulated probability density functions (PDF) for the top section of the column [420–600 mm]. The distributions demonstrate a very good match considering the simple model that was employed for the bubble cutting by the wire mesh.

The pH decay curves for the six stage multiple-mesh configuration are shown in Fig. 13c. The pH trends and reaction times are fairly well predicted by the VoF-DBM model as compared with the experiments. Fig. 13d shows the gas holdup vs time curves for the multiple-mesh configuration with six stages. The gas holdup is slightly over-predicted during the course of the reaction. The expected increase in gas holdup that is due to bubble cutting, is well captured in the simulations.

5. Conclusions

In this work, a detailed analysis of the micro-structured bubble column (MSBC) has been performed for the case of chemisorption of CO_2 into NaOH. Different internals such as a wire mesh and a Sulzer packing (SMV) have been tested in the MSBC experimentally to characterize the bubble cutting and mass transfer performance.

The Sulzer packing and the wire mesh with a 3.7 mm opening shows good cutting characteristics as seen in their bubble size distribution. This increases the interfacial area in turn resulting in an increased gas holdup and better mass transfer performance. Since the chemisorption is mass transfer limited the reaction times are found to decrease significantly in presence of the internals. The multiple-mesh configuration with six staged meshes is seen to have a better performance than a single mesh due to the increased bubble cutting and gas holdup. The performance of the multiple-mesh configuration with ten stages is hindered by the decrease in back-mixing and reduction in mass transfer due to bubble swarm effects.

The VoF-DBM model is integrated with equations for chemisorption and validated with experiments. An optimal value of the cutting efficiency was determined and the simulation results are compared with experiments. The major drawback of the cutting model is that it is independent of the superficial gas velocity. Therefore an effort should be made to improve the cutting model by using closures from direct numerical simulations (DNS).

Acknowledgements

References

Allen, M.P., Tildesley, D.J., 1989. Computer simulation of liquids. Oxford University Press.

Baird, M.H.I., 1992. Bubble column reactors. By W.D. Deckwer, Wiley, New York, 1991. AIChE J. 38 (8), pp. 1305–1305.

Brauer, H., 1981. Particle/fluid transport processes. Prog. Chem. Eng. 19, 81–111.

Darmana, D., Deen, N.G., Kuipers, J.A.M., 2005. Detailed modeling of hydrodynamics, mass transfer and chemical reactions in a bubble column using a discrete bubble model. Chem. Eng. Sci. 60 (12), 3383–3404. Jun..

Deen, N.G., Mudde, R.F., Kuipers, J.A.M., Zehner, P., Kraume, M., 2000. Bubble Columns. Wiley-VCH Verlag GmbH & Co.

Jain, D., Kuipers, J., Deen, N.G., 2015. Numerical modeling of carbon dioxide chemisorption in sodium hydroxide solution in a micro-structured bubble column. Chem. Eng. Sci. 137, 685–696.

Jain, D., Kuipers, J.A.M., Deen, N.G., 2014. Numerical study of coalescence and breakup in a bubble column using a hybrid volume of fluid and discrete bubble model approach. Chem. Eng. Sci. 119, 134–146. Nov..

Jain, D., Lau, Y.M., Kuipers, J.A.M., Deen, N.G., 2013. Discrete bubble modeling for a micro-structured bubble column. Chem. Eng. Sci. 100, 496–505. Aug..

Lau, Y.M., Deen, N.G., Kuipers, J.A.M., 2013a. Development of an image measurement technique for size distribution in dense bubbly flows. Chem. Eng. Sci. 94, 20–29. May.

Lau, Y.M., Sujatha, K.T., Gaeini, M., Deen, N.G., Kuipers, J.A.M., 2013b. Experimental study of the bubble size distribution in a pseudo-2D bubble column. Chem. Eng. Sci. 98, 203–211. Jul..

Meyer, F., 1994. Topographic distance and watershed lines. Signal Process. 38 (1), 113–125. Jul..

Otsu, N., 1975. A threshold selection method from gray-level histograms. Automatica 11 (285–296), 23–27.

Prince, M.J., Blanch, H.W., 1990. Bubble coalescence and break-up in air-sparged bubble columns. AIChE J. 36 (10), 1485–1499.

Sommerfeld, M., Bourloutski, E., Bröder, D., 2003. Euler/Lagrange calculations of bubbly flows with consideration of bubble coalescence. Can. J. Chem. Eng. 81 (3–4), 508–518.

Sujatha, K.T., Meeusen, B.G.J., Kuipers, J.A.M., Deen, N.G., 2015. Experimental studies of bubbly flow in a pseudo-2D micro-structured bubble column reactor using digital image analysis. Chem. Eng. Sci. 130, 18–30.

van Sint Annaland, M., Deen, N.G., Kuipers, J.A.M., 2005. Numerical simulation of gas bubbles behaviour using a three-dimensional volume of fluid method. Chem. Eng. Sci. 60 (11), 2999–3011. Jun..

Vreman, A.W., 2004. An eddy-viscosity subgrid-scale model for turbulent shear flow: algebraic theory and applications. Phys. Fluids 16 (10), 3670.

Westerterp, K.R., Van Swaaij, W.P.M., Beenackers, A., 1987. Chemical Reactor Design and Operation, vol. 84. Wiley, Chichester.